A Simultaneous Numerical Solution for the Lubrication and Dynamic Stability of Noncontacting Gas Face Seals

Itzhak Green
George W. Woodruff
School of Mechanical Engineering,
Georgia Institute of Technology,
Atlanta, GA 30332-0405

Roger M. Barnsby
Pratt and Whitney,
United Technologies Corporation,
East Hartford, CT 06108

A numerical solution is presented for the dynamic analysis of gas lubricated noncontacting mechanical face seals having a single grounded flexibly mounted stator. Seal dynamics is solved in axial and angular modes of motion. Both the Reynolds equation and the equations of motion are arranged into a single state space form, allowing the fluid film lubrication and the dynamics to be solved simultaneously. The resulting set of equations is solved using a high-order multistep ordinary differential equation solver, yielding a complete simulation for the seal dynamic behavior. Examples of seal motion are given in detailed transient responses. The stability threshold is investigated to gauge the influence of seal parameters such as inertia, speed, coning, and the direction of sealed pressure drops. The results show two modes of instability: (1) When the inertia effect is larger than a critical value, the natural response of the seal grows monotonically in a half-frequency-whirl mode. (2) When the seal coning is less than some critical value in an outside pressurized seal, the minimum film thickness diminishes because of hydrostatic instability, and face contact occurs. Conversely, an inside pressurized seal is shown to be hydrostatically stable and have a superior dynamic response at any coning.
[DOI: 10.1115/1.1308020]

Introduction

Gas lubricated mechanical face seals can be found in many applications of high speed turbomachinery, e.g., air compressors, turbopumps, turbofan, and turbojet engines. Yet the body of work on the dynamics of mechanical face seals concerns primarily liquid lubricated seals [1–3]. For example, Green and Etsion [4] obtained expressions for the stiffness and damping of liquid lubricated, coned face seals. Using some simplifying assumptions, the lubrication equation could be solved analytically, yielding stiffness and damping (rotordynamic) coefficients, which were completely decoupled from the dynamic equations. This decoupling subsequently aided in the development of a general closed form solution for the dynamics of any coned face mechanical seal [5]. The equations of motion were solved analytically, giving criteria for stability and expressions for steady-state responses to rotor runout and static stator misalignment.

While the geometry of motion (i.e., the seal kinematics) is independent of the type of lubrication, due to compressibility and pressure nonlinearity gas seal dynamic analysis differs significantly from a liquid seal analysis. Specifically, universal closed-form expressions for the stiffness and damping of pressurized coned face gas seals are not available. Forces and moments in a gas film depend not only on the instantaneous kinematical state but also upon the history of motion. The lubrication analysis thus must be coupled with the dynamics of the face seal. Therefore, even to date, a full numerical simulation is the sole method available for the dynamic analysis of gas face seals.

Because of the low gas viscosity, some gas seal designs feature lifting mechanisms in the sealing dam (e.g., Raleigh steps, waves, spiral grooves) that generate elevated hydrodynamic pressures to facilitate noncontacting operation. However, many gas seal designs retain the simplicity of flat faces. The understanding of how such seals can operate satisfactorily would be beneficial.

It is the intent of this study to provide a solution such that the mutual interaction between the gas film and the dynamics of the seal are solved simultaneously. The numerical solution presented here is unique because numerical solutions in the past (Cha and Bogy [6]; Leefe [7]; Shapiro and Colsher [8]; Castelli and Pirvics [9]) have been split into two separate steps: within every time instant the lubrication equation was solved ''quasistatically'' to give forces and moments. These were then placed in the equations of motion and the time integration of the dynamic equation was forwarded. The coupling accomplished through this method is really a piecewise procedure requiring a very time consuming and repeated solution of the lubrication problem at every instant of time [8]. From a strict mathematical point of view, such procedures bypass the real problem because the solution does not evolve simultaneously.

The technique presented here systematically couples the lubrication and kinetic equations for face seals so that they are solved simultaneously. This technique draws on the principles outlined in the following works: (1) Green and Etsion [5,10] provided closed-form and nonlinear numerical solutions for the dynamics of coned face seals with incompressible fluids. Because of fluid incompressibility, both works justifiably embraced a closed form solution of the Reynolds equation. This work cannot assume such a solution because of fluid compressibility. However, the seal kinematics outlined there can be fully adopted here. (2) The unique method of the solution for the coupled system of lubrication and dynamic follows the procedure outlined by Miller and Green [11]. The present work, however, differs in two aspects: (i) Miller and Green give the solution in an inertial coordinate system; here the solution is provided in a rotating (whirling) coordinate system; (ii) Miller and Green outline the solution using finite element and finite volume techniques that handle spiral groove discontinuities; here the solution is reached using a finite difference technique that efficiently handles flat faces. The coupled equations are framed in a state space form and solved numerically by efficient high order,

Contributed by the Tribology Division of THE AMERICAN SOCIETY OF MECHANICAL ENGINEERS for presentation at the STLE/ASME Tribology Conference, Seattle, WA, October 1–4. Manuscript received by the Tribology Division Feb. 7, 2000; revised manuscript received June 8, 2000. Paper No. 2000-TR1B-10. Associate Editor: J. Frêne.

multistep ordinary differential equation solvers [12]. The technique is used to find the seal natural response to an initial condition disturbance for a reference case, and then to investigate how varying some parameters affects seal stability.

Formulation of a Simultaneous Solution

Figure 1 shows the schematic of a mechanical seal having a flexibly mounted stator configuration. It consists of a seal seat (rotor) that is rigidly mounted to the rotating rigid shaft, and a flexibly supported seal ring (stator). The rotor misalignment is represented by a tilt γ_r measured between the out normal to its plane and the axis of shaft rotation (see Fig. 2). Similarly, the stator may have an initial misalignment γ_{si} with respect to the axis of shaft rotation. At rest, and with zero-pressure differential, the stator is pressed against the rotor by the supporting springs to assume the same tilt, γ_r, as that of the rotor. During operation, however, the mating faces separate and the stator assumes its own tilt, γ_s.

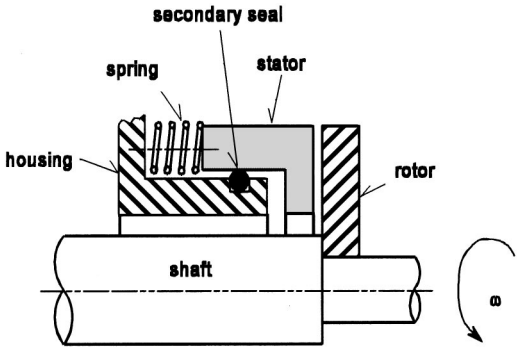

Fig. 1 Schematic of noncontacting mechanical face seal

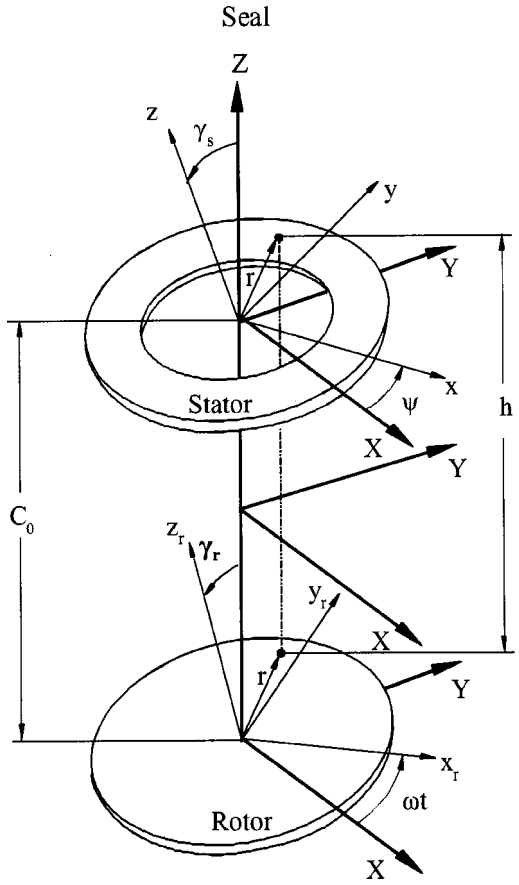

Fig. 2 Seal kinematical model

Stability specifically deals with the natural response of the system where all forcing functions have been removed, mathematically expressed as $\gamma_r = \gamma_{si} = 0$, which leaves homogeneous equations of motion. When a closed form solution is possible, a characteristic equation is formulated and investigated. Frequently, conditions are imposed to guarantee that the eigenvalues contain a diminishing effect upon the natural response. In other words, a stable system is such that when a disturbance excites the system, its tendency is to diminish and eliminate the disturbance, consequently returning the system to its normal operation. Conversely, an unstable system will undergo large dynamic excursions from its designed point, resulting in large stator tilts that will cause face contact and excessive leakage, i.e., seal failure.

Without rotor misalignment the local film thickness (shown in Fig. 2) is expressed in an inertial frame

$$h = C_o + Z + \beta(r - r_i) - \gamma_s r \sin(\psi - \theta) \tag{1}$$

where C_o is the designed centerline clearance and β is the face coning (see Fig. 3). The stator degrees of freedom are the axial displacement, Z, the nutation, γ_s, and the precession, ψ (see Fig. 2). The equations of motion are expressed in a whirling frame (see Green and Etsion [5]):

$$I(\ddot{\gamma}_s - \dot{\psi}^2 \gamma_s) = M_x \tag{2}$$

$$I(\ddot{\psi}\gamma_s + 2\dot{\psi}\dot{\gamma}_s) = M_y \tag{3}$$

$$m\ddot{Z} = F_Z \tag{4}$$

where M_x and M_y are, respectively, the moments acting on the stator about axes x and y, which belong to a coordinate system xyz that whirls at a rate $\dot{\psi}$ within an inertial system XYZ (see Fig. 2). The tilt vector $\vec{\gamma}_s$ takes place about axis x of the rotating system,

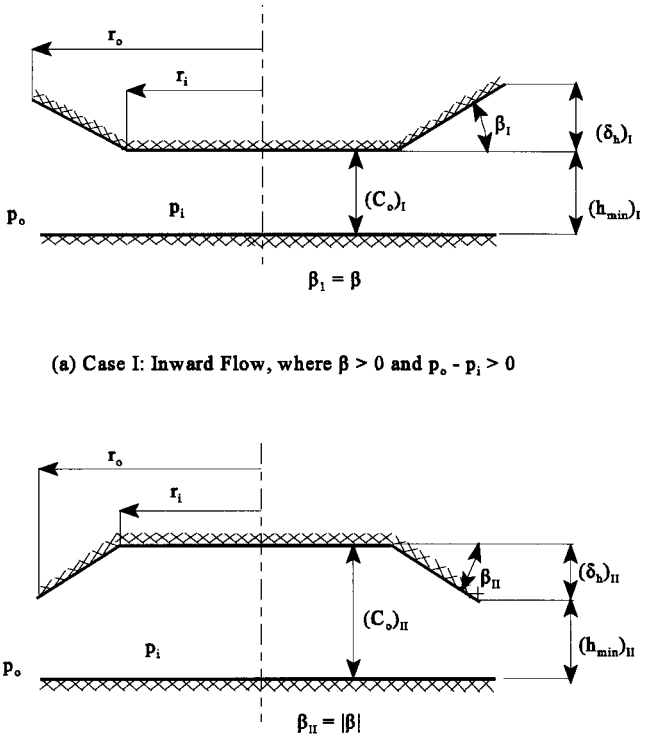

Fig. 3 Schematic of coning in inward and outward flow regimes

which is positioned by an angle ψ with respect to the inertial axis X. The moments M_x and M_y, and the axial force F_Z consist of contributions from both the flexible support and the fluid film. The support moments and force are

$$M_{sx} = -K_s \gamma_s - D_s \dot{\gamma}_s \tag{5}$$

$$M_{sy} = -D_s \dot{\psi} \gamma_s \tag{6}$$

$$F_{sZ} = -K_{sZ} Z - D_{sZ} \dot{Z} \tag{7}$$

where K_{sZ} and D_{sZ} are, respectively, the axial stiffness and damping coefficients of the support. These coefficients include the dynamic properties of the supporting springs and the secondary seal, which can be metal bellows, piston rings, elastomeric O-rings, etc. Typically the dynamic properties of the secondary seals need to be determined experimentally (e.g., Green and Etsion [13], Lee and Green [14]). From the measured coefficients K_{sZ} and D_{sZ}, the angular stiffness and damping coefficients K_s and D_s can be calculated according to Green and Etsion [5].

The fluid film contribution to M_x, M_y, and F_Z is obtained by numerically integrating the pressure distribution in the sealing dam over the face area. The gas flow is assumed to be isothermal, isoviscous, and ideal; therefore, it is governed by the compressible form of the Reynolds equation (e.g., Gross [15]),

$$\frac{\partial p}{\partial t} = \vec{\nabla} \cdot \left[\frac{p h^3 \vec{\nabla} p}{12 \mu} - \frac{1}{2} \omega r p h \vec{i}_\theta \right] - \frac{\partial h}{\partial t} \tag{8}$$

where the operator $\vec{\nabla}$ is implied here in inertial cylindrical coordinates r and θ, and $p = p(r, \theta, t)$. This equation is subject to the boundary conditions (B.C.):

$$\begin{aligned} p(r_i, \theta, t) &= p_i \\ p(r_o, \theta, t) &= p_o \\ p(r, 0, t) &= p(r, 2\pi, t) \end{aligned} \tag{9}$$

where p_i and p_o are the inner and outer pressures. The last equation represents a cyclic B.C.; it is necessary here because a stator angular response will require a nonaxisymmetric pressure solution over the entire sealing dam as the simulation progresses in time. Equation (8) is already written in a form suitable for the state space formulation outlined subsequently. Specifically, the Reynolds equation is discretized in a finite difference scheme where the pressures in the sealing dam are referenced in a state space vector form.

In addition to the B.C. specified in Eq. (9) the initial condition (I.C.) for the pressure must also be specified. To obtain the initial pressure conditions, the Reynolds equation is solved with the transient terms in Eq. (8) set to zero. Also, without forcing misalignments the stator initially is perfectly aligned, resulting in axisymmetric conditions at $t = 0$. Hence, the Reynolds equation degenerates to

$$\frac{\partial}{\partial r} \left(r p h^3 \frac{\partial p}{\partial r} \right) = 0 \tag{10}$$

subject to the same B.C. as in Eq. (9). The appendix details the solution for Eq. (10), which symbolically can be written as

$$p(r, \theta, 0) = p_{\mathrm{IC}}(r, \theta) \tag{11}$$

where p_{IC} is the initial condition of the pressure as given by Eq. (*A*8). At every instant of time the fluid film moments and force M_{fx}, M_{fy}, and F_{fZ} are obtained by numerically integrating the pressure over the dam area, having the moments calculated about the whirling x and y axes:

$$M_{fx} = \int_0^{2\pi} \int_{r_i}^{r_o} p r^2 \sin(\theta - \psi) dr \, d\theta \tag{12}$$

$$M_{fy} = -\int_0^{2\pi} \int_{r_i}^{r_o} p r^2 \cos(\theta - \psi) dr \, d\theta \tag{13}$$

$$F_Z = \int_0^{2\pi} \int_{r_i}^{r_o} p r \, dr \, d\theta \tag{14}$$

Since Z, γ_s, and ψ are time dependent then h, p, M_{fx}, M_{fy}, and F_Z are all time dependent as well. The equations of motion (2)–(4) are recast now in a state space form including the support and fluid film effects,

$$\frac{\partial}{\partial t} \begin{Bmatrix} \dot{Z} \\ Z \\ \dot{\gamma}_s \\ \gamma_s \\ \dot{\psi} \\ \psi \end{Bmatrix} = \begin{Bmatrix} (F_{sZ} + F_{fZ})/m \\ \dot{Z} \\ (M_{sx} + M_{fx})/I + \dot{\psi}^2 \gamma_s \\ \dot{\gamma}_s \\ [(M_{sy} + M_{fy})/I - 2\dot{\psi}\dot{\gamma}_s]/\gamma_s \\ \dot{\psi} \end{Bmatrix} \tag{15}$$

subject to the initial conditions $Z(0)$, $\dot{Z}(0)$, $\gamma_s(0)$, $\dot{\gamma}_s(0)$, $\psi(0)$, $\dot{\psi}(0)$.

Now suppose that the finite difference discretization of the Reynolds equation contains *nr* by *nth* nodes in the radial and circumferential directions, respectively. Hence, excluding the pressure boundary conditions, a large state vector $\{\varphi\}$ is formed with a dimension of $(nr-2)*nth+6$. The first $(nr-2)*nth$ elements are allocated for the time derivatives of interior nodal pressures as stated by Eq. (8), and the last six elements are allocated for the degrees of freedom in the state vector of Eq. (15). This forms an explicit general system of equations

$$\frac{\partial}{\partial t} \{\varphi\} = \{\mathrm{RHS}\} \tag{16}$$

where {RHS} is a column vector containing the right-hand-side of the relevant equation, i.e., either Eq. (8) or Eq. (15). This form contains the time dependent parameters of all variables coupled in a single system suitable for integration by multistep ordinary differential equation solvers employing the Adams-Moulton and Gear's backward differentiation formula [12]. It is worthy of note that the kinematical variables (i.e., degrees of freedom) that need to be solved for in Eq. (15) are implicitly included in Eq. (8) by means of Eq. (1). Conversely, the pressures obtained from Eq. (8) at every instant of time are needed in the calculation of force and moments that appear in Eq. (15). In other words, Eq. (1) is the source of coupling. The solution of Eq. (16) gives a simultaneous dynamic simulation for the transient pressure as well as for all the kinematical variables, i.e., the seal motion.

Stability Analysis

A base case is investigated for two possibilities of support effects: (1) with support stiffness and damping coefficients given in Table 1, and (2) with the same parameters but with no support effects. The investigation is performed first by changing the speed between runs. The initial conditions are such that the stator and rotor are perfectly aligned, i.e., for axisymmetric conditions at $t = 0$, we specifically set $Z(0) = \gamma_s(0) = 0$. The other I.C. are chosen as $\dot{Z}(0) = \psi(0) = 0$, $\dot{\psi}(0)/\omega = 1$. The seal is set into motion (i.e., being perturbed) by a tilt (nutation) velocity, $\dot{\gamma}_s(0)(r_o/C_o)/\omega = 0.5$. A finite difference mesh of $nr = 9$ and $nth = 253$ is used initially. Then a finer mesh with $nr = 11$ and $nth = 313$ is found to produce practically indistinguishable results, thus confirming mesh convergence. All the data presented here is taken from simulations that used the finer mesh.

Response plots of the base case at five different speeds are shown in Fig. 4. The plots are shown in a nondimensional form: the stator tilt, γ_s is normalized by C_o/r_o, and the minimum film thickness, $h_{\min}$ [i.e., the minimum value of Eq. (1)] is normalized by C_o. The axial displacement Z behaves similarly to γ_s and,

Table 1 Seal base cases

ω=2094.4 rad/s	(ω=20,000 rpm)
μ=1.8 (10)$^{-5}$ Pa·s,	C_o=6 μm
p_i = 1 (10)^5 Pa	p_o = 2 (10)^5 Pa
r_i = 0.048 m	r_o= 0.06 m
β = 0.25 mrad	(δ_h = 3 μm)
m= 1 kg	I= 0.0018 kg·m^2
case 1: K_s= 5 (10)^5 N/m	D_s= 300 N s/m
case 2: K_s= 0 N/m	D_s= 0 N s/m

therefore, is not plotted. Time is normalized by ωt, yielding the shaft revolution since $t=0$. Since this is an exhaustive search, a very large number of runs would be required to pinpoint exactly the stability threshold. First, however, the area of instability is found by trial and error. Then five cases are allowed to vary by 10 rad/s to approximate closely the neighborhood of instability within ± 5 rad/s, or within an uncertainty of the order of ±0.1 percent. First, all five cases exhibit initial oscillatory transients that decay rapidly within the first two revolutions (see insets in Fig. 4). Then monotonic behavior prevails thereafter and throughout 100 revolutions of simulation. Speeds at or above 3020 rad/s exhibit diverging responses, where γ_s increases monotonically, causing $h_{\min}$ to decrease monotonically. In other words, the seal is

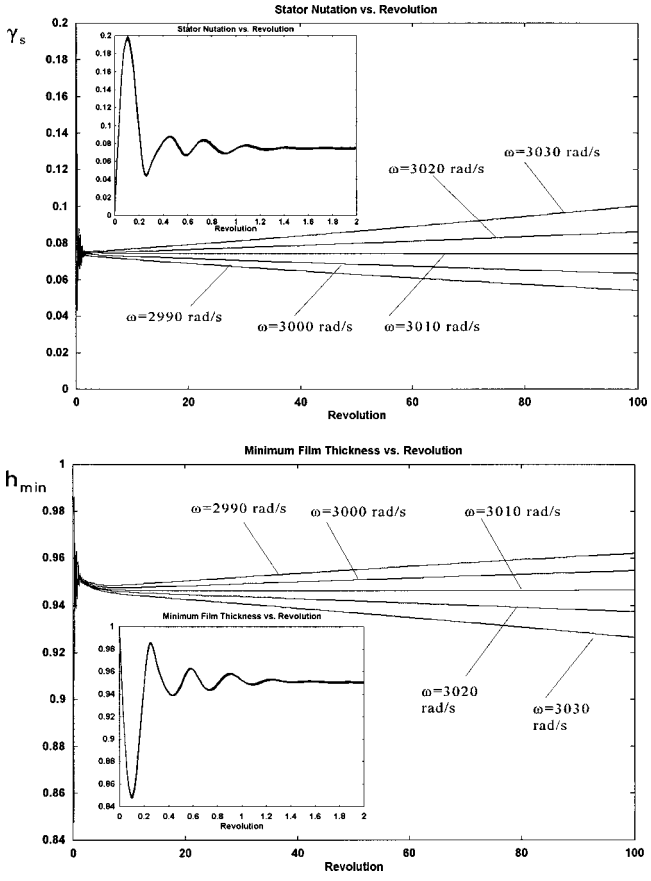

Fig. 4 Transient dynamic response at various shaft speeds

dynamically unstable, because if a sufficiently large time is allowed, the faces would eventually come into contact (wear would occur and the leakage would likely be intolerable). Conversely, speeds at or below 3000 rad/s exhibit stable operation, where the faces get realigned and $h_{\min}$ approaches its designed value of C_o. At the speed of 3010 rad/s it is clear that after the initial transient, the response does not grow nor does it diminish in time. It is concluded that a speed of 3010 rad/s is the critical speed of instability in this case. The data also reveals that at the stability threshold the stator whirls in a subsynchronous mode having $\dot{\psi}/\omega_{\rm cr} = 0.4924$, i.e., slightly lower than a half-frequency whirl. A similar exhaustive search is performed but with $K_s = D_s = 0$. Without showing the plots, the critical speed is found to be nearly 2600 rad/s (having the same uncertainty as above). Here, however, $\dot{\psi}/\omega_{\rm cr} = 0.5000$, indicating precisely a half-frequency whirl mode. The results are summarized in Table 2, along with the CPU time for executing 100 revolutions on a 550 MHz PC. The immediate conclusion is that support stiffness and damping are beneficial for increasing the value of the critical speed.

Comparing this study ''half-frequency whirl mode'' at the stability threshold for a compressible film, to the case where the film is incompressible (see the closed-form solution by Green and Etsion [5]) reveals indeed that in both studies: (1) stiffness and damping of the support increase the critical speed, and (2) the whirl at the stability threshold is at or about ''half-frequency'' where support damping decreases the value of the whirl frequency. These findings add credibility to the simultaneous numerical solution outlined above.

Another exhaustive search is conducted. The speed is now held constant at 2094.4 rad/s (20,000 rpm), but the inertia properties are varied. With support effects it is discovered that the stability threshold occurs at about $m = 2.0654$ kg, and $I = 3.7178 \times 10^{-3}$ kg m^2. Calculating now at the inertia product of $I \cdot \omega^2$ at stability threshold gives $I \cdot \omega^2 = 16{,}309$ *J*. Likewise, for the second case where $K_s = D_s = 0$ the seal stability threshold occurs at about $m = 1.5411$ kg, and $I = 2.774 \times 10^{-3}$ kg m^2, or $I \cdot \omega^2 = 12{,}175$ *J*. These critical inertia products are very close to the values calculated for the cases when the speed is varied and mass is held constant (16,308 *J* and 12,168 *J*, respectively, see Table 2). Apparently what really matters for the stability threshold is the critical inertia product $(I \cdot \omega^2)_{\rm cr}$. While this term has units of energy, the product is of the stator transverse moment of inertia (about axes *x* and *y*) with the shaft speed that takes place about axis *Z*; hence, this should not be confused with the kinetic energy of the stator. Again, this phenomenon is entirely consistent with the closed-form solution for incompressible seals (Green and Etsion [5]). Only here, because a closed form solution for stiffness and damping cannot be obtained for a compressible film, the stability threshold must be found in this arduous empirical way.

An important parameter for seal stability is face coning. In order not to mask stability characteristics by support effects, the second case in Table 1 is run with coning angles varying from zero to 0.25 mrad (or taper heights δ_h from zero to 3 μm). Figure 5 shows the transient response for six cases of coning, plotting the normalized misalignment and the minimum film thickness versus shaft revolution. Figure 5 demonstrates that the seal response is stable when the taper height is at or above 2.5 μm, having responses that diminish in time and that restore the stator tilt to a perfectly aligned condition, $\gamma_s = 0$. Also, the minimum film thickness restores its value at the design clearance. On the other hand, the seal exhibits an unstable response when the taper height is at or below 2.0 μm, where the stator tilt diverges quite rapidly, eventually causing face contact, i.e., $h_{\min} = 0$. An arduous trial and error procedure would be needed again to pinpoint exactly the critical coning at the stability threshold. However, the critical value would clearly be somewhere between taper heights of 2.0 and 2.5 μm. These correspond to coning angles of 0.167 and 0.208 mrad, respectively, which when normalized by C_o/r_o result in 1.67 and 2.08. Green and Etsion [5] determined analytically a

Table 2 Critical parameters determined at stability threshold

Reference value held constant in simulation	Base case with support effects K_s= 5 (10)^5 N/m D_s= 300 N s/m		Base case without support effects K_s= 0 N/m D_s= 0 N s/m	
m=1 kg $I = 1.8\cdot10^{-3}$ kg·m^2	ω_{cr} =3010 rad/s $\dot{\psi}/\omega_{cr}$ = 0.4924 (CPU= 56 min)	$I\cdot\omega_{cr}^2$ =16308 J	ω_{cr} =2600 rad/s $\dot{\psi}/\omega_{cr}$ = 0.5 (CPU=33 min)	$I\cdot\omega_{cr}^2$ =12168 J
ω = 2094.4 rad/s	m_{cr}=2.065 kg $I_{cr} = 3.718\cdot10^{-3}$ kg·m^2 (CPU= 45 min)	$I_{cr}\cdot\omega^2$ =16309 J	m_{cr}=1.542 kg $I_{cr} = 2.776\cdot10^{-3}$ kg·m^2 (CPU= 43 min)	$I_{cr}\cdot\omega^2$ =12175 J

nondimensional critical coning angle of r_o/r_i (here $r_o/r_i = 1.25$), but this value is only valid for incompressible seals. The latter would be an underestimation and, therefore, an unsafe value for compressible seals. This sort of instability is caused rather by hydrostatic effects and not by inertia effects. Nevertheless, the phenomenon that a critical coning angle exists, prevails in compressible and incompressible seals alike. All the above pertains to seals pressurized on the outside radius causing inward flow, as shown in Fig. 3(*a*).

To gauge the effects of seals pressurized on the inside radius and causing outward flow, similar cases have been simulated but with the pressures in Table 1 reversed, i.e., $p_i = 2\times10^5$ Pa, and $p_o = 10^5$ Pa. The designed seal clearance is unchanged and maintained at 6 μm, but now the gap is converging with the radial direction to impose flow in a converging gap [see Fig. 3(*b*)]. The simulation results are shown in Fig. 6 with negative taper heights

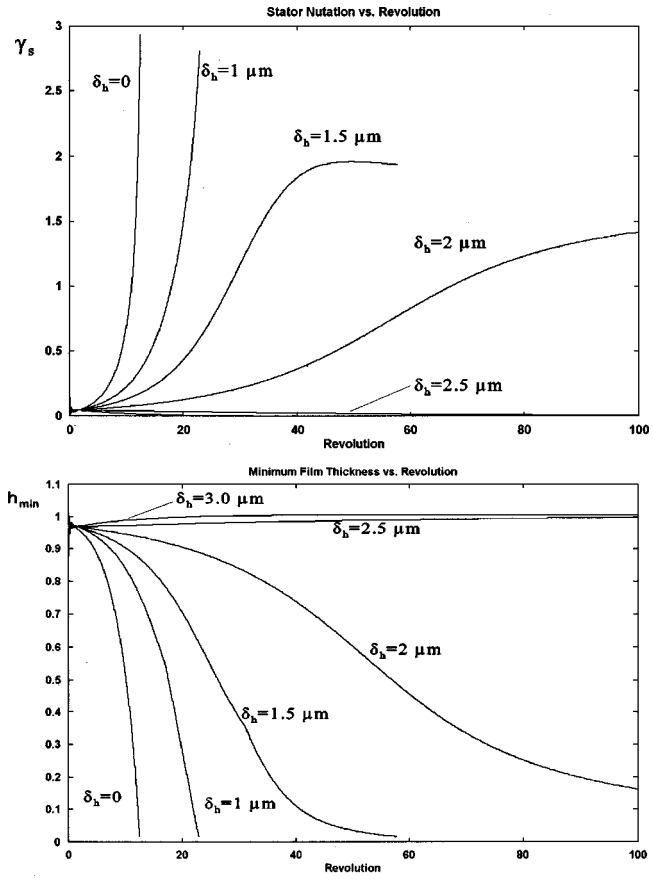

Fig. 5 Transient response for an outside pressurized seal (inward flow) at various positive coning angles

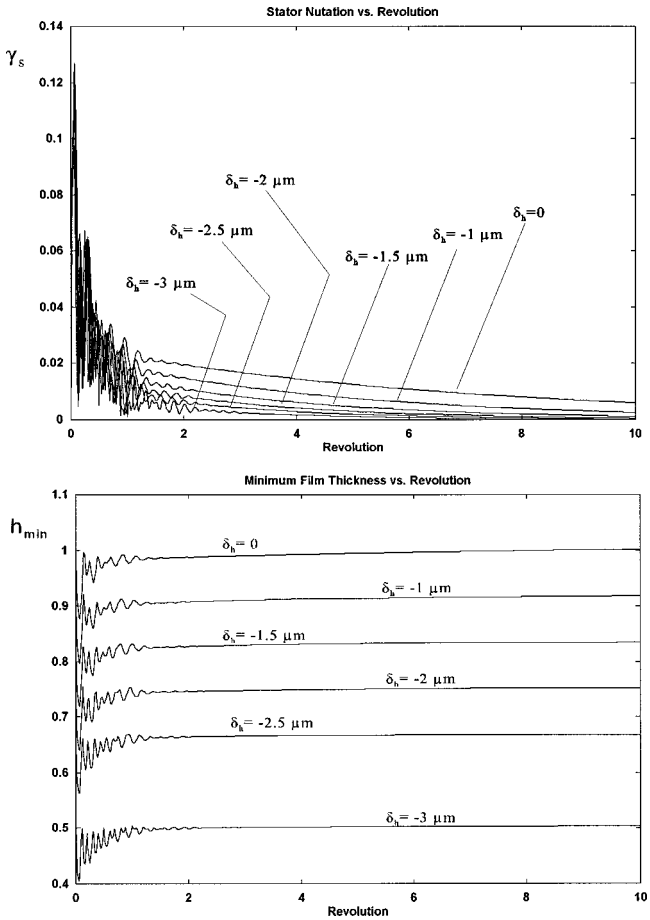

Fig. 6 Transient response for an inside pressurized seal (outward flow) at various negative coning angles

having the same absolute magnitudes as previously. Obviously, the transient responses shown in Fig. 6 are very different in nature from those shown in Fig. 5. First, all negative coning angles produce stable dynamic behaviors when the high pressure is at the inside radius. Even the zero coning situation is stable in the angular mode, but it should be avoided (see discussion by Green [16]). The simulations continued for 100 revolutions, but the transient response diminished rather quickly, so only 10 revolutions are shown. It can be seen that following initial high-frequency oscillations the responses settle in a monotonic decay to stable and perfectly aligned conditions. The higher the face coning the faster the decaying response. This behavior must be the result of higher angular film stiffness, a characteristic consistent with the findings by Green [16]. The minimum film thickness is reduced because the faces converge in the radial direction; hence, since $h_{\min}$ occurs at the outer radius the normalized steady-state value is also reduced. In summary, this type of seal (outward flow) is proven to be dynamically superior compared with the previous type (inward flow), because (i) it does not suffer from hydrostatic instabilities, (ii) while an inside pressurized seal is still prone to dynamic instability, it possesses a higher angular film stiffness which would result in a higher critical inertia value of $(I\cdot\omega^2)_{\rm cr}$. Thermal effects, however, tend to open up the film in the radial direction. Such effects must be minimized in order to capture the dynamic superiority of this type of mechanical face seal. The stability investigation is only the first and necessary step in a complete dynamic analysis. Once a seal is determined to be stable, the steady-state analysis must follow. That is, we must determine how the stator tracks a misaligned rotor in the presence of an initially misaligned stator.

Conclusions

A twofold objective is attained: (I) First, a new numerical formulation is given where the Reynolds equation and the equations of motion are arranged into a single state space form; this formulation allows the fluid film lubrication and the dynamics to be solved concurrently. The resulting set of equations is integrated simultaneously using efficient multistep ordinary differential equation solvers yielding a complete simulation for the seal dynamic behavior in all of its kinematical variables. (II) Then using the new formulation a numerical solution is presented for the stability analysis of noncontacting gas face seals. Base cases are investigated by inspection, where the complete transient responses are searched for instabilities. A critical inertia term, $(I\cdot\omega^2)_{\rm cr}$, empirically emerges above whose value seals become dynamically unstable, with the natural response growing monotonically in a subsynchronous half-frequency whirl mode. For a flexibly mounted stator seal, support effects help in raising this critical inertia value. It is also empirically found that in order to avoid hydrostatic instability an outside pressurized seal must possess a coning angle greater than critical; otherwise the seal lubricating gas film diminishes and face contact occurs. However, inside pressurized seals do not suffer from hydrostatic instabilities at any convergent coning. Moreover, added convergent coning improves the dynamic behavior even further.

Nomenclature

C = centerline clearance
C_o = design clearance
D_Z = axial damping coefficient
D = angular damping coefficient
F = force
h = local film thickness
I = transverse moment of inertia
K_Z = axial stiffness coefficient
K = angular stiffness coefficient
M = moment
M_{Xi} = moment due to stator initial misalignment
m = stator mass
p = pressure
r = radial coordinate
t = time
Z = axial degree of freedom
β = face coning angle, $\delta_h/(r_o-r_i)$
γ_r = rotor runout
γ_s = stator nutation
γ_{si} = stator initial misalignment
δ_h = coning (taper) height
θ = angular coordinate
μ = viscosity
ψ = precession
ω = shaft angular velocity

Subscripts

cr = critical
f = fluid film
i = inner radius
o = outer radius
r = rotor
s = stator, or flexible support

Appendix-Solution of the Compressible Reynolds Equation for Axisymmetric Coned Seals

Equation (10) is recast here in an alternate (but mathematically equivalent) form

$$\frac{\partial}{\partial r}\left(rh^3\frac{\partial p^2}{\partial r}\right)=0 \tag{A1}$$

subject to the B.C.

$$p^2(r_i)=p_i^2$$
$$p^2(r_o)=p_o^2 \tag{A2}$$

It can be seen that the solution is carried out on p^2 rather than on p itself, because a solution to Eq. (A1) can be obtained in closed form. Imposing the axisymmetric condition on the film thickness expressed in Eq. (1), with the initial conditions $Z(0)=\gamma_s(0)=0$, gives

$$h=C_o+\beta(r-r_i)\equiv a+\beta r;\quad a=C_o-\beta r_i \tag{A3}$$

Also define conveniently

$$h(r=r_i)=C_o\equiv h_i$$
$$h(r=r_o)=C_o+\beta(r_o-r_i)\equiv h_o \tag{A4}$$

Substituting (A3) in (A1) and integrating (A1) twice results in

$$p^2=c_1\frac{a+2h}{(ah)^2}+2c_1\frac{\ln r-\ln h}{a^3}+c_2 \tag{A5}$$

where c_1 and c_2 are constants of integration determined by using the B.C. in Eq. (A2) along with the definitions of (A4). Hence,

$$c_1=\frac{p_i^2-p_o^2}{\dfrac{1}{ah_i^2}-\dfrac{1}{ah_o^2}}+\frac{2\left(\dfrac{1}{h_i}-\dfrac{1}{h_o}\right)}{a^2}+\frac{2\left[\ln\left(\dfrac{r_i}{r_o}\right)-\ln\left(\dfrac{h_i}{h_o}\right)\right]}{a^3} \tag{A6}$$

$$c_2=p_i^2-c_1\frac{a+2h_i}{a^2h_i^2}+2\,\frac{\ln r_i-\ln h_i}{a^3} \tag{A7}$$

From Eq. (A5) we have

$$p_{\rm IC}=\sqrt{c_1\frac{a+2h}{(ah)^2}+2c_1\frac{\ln r-\ln h}{a}+c_2} \tag{A8}$$

which upon substitution of (A6) in (A7), and then substituting both in (A8) gives finally the solution for the pressure. Although (A8) does not provide an explicit expression for the pressure, it is nev-

ertheless a closed-form solution that can easily be computed. This solution is taken as the initial condition for the pressure in the sealing dam, thus carrying the subscript IC.

References

[1] Etsion, I., 1982, ''A Review of Mechanical Face Seal Dynamic,'' Shock Vibr. Dig., **14**, No. 3, pp. 9–14.

[2] Etsion, I., 1985, ''Mechanical Face Seal Dynamics Update,'' Shock Vibr. Dig., **17**, No. 4, pp. 11–16.

[3] Etsion, I., 1991, ''Mechanical Face Seal Dynamics 1985–1989,'' Shock Vibr. Dig., **23**, No. 4, pp. 3–7.

[4] Green, I., and Etsion, I., 1983, ''Fluid Film Dynamic Coefficients in Mechanical Face Seals,'' ASME J. Lubr. Technol., **105**, No. 2, pp. 297–302.

[5] Green, I., and Etsion, I., 1985, ''Stability Threshold and Steady-State Response of Noncontacing Coned-Face Seals,'' ASLE Trans., **28**, No. 4, pp. 449–460.

[6] Cha, E., and Bogy, D. B., 1995, ''A Numerical Scheme for Static and Dynamic Simulation of Subambient Pressure Shaped Rail Sliders,'' ASME J. Tribol., **117**, pp. 36–46.

[7] Leefe, S., 1994, ''Modeling of Plain Face Gas Seal Dynamics,'' *14th International Conference on Fluid Sealing*, BHR Group Conference Series, No. 9, pp. 397–424.

[8] Shapiro, W., and Colsher, R., 1974, ''Steady State and Dynamic Analysis of a Jet-Engine, Gas Lubricated Shaft Seal,'' ASLE Trans., **17**, No. 3, pp. 190–200.

[9] Castelli, V., and Pirvics, J., 1968, ''Review of Numerical Methods in Gas Bearing Film Analysis,'' ASME J. Lubr. Technol., **90**, pp. 777–792.

[10] Green, I., and Etsion, I., 1986, ''Nonlinear Dynamic Analysis of Noncontacting Coned-Face Mechanical seals,'' ASLE Trans., **29**, No. 3, 383–393.

[11] Miller, B., and Green, I., 1999, ''Numerical Formulation for the Dynamic Analysis of Spiral-Grooved Gas Face Seals,'' presented at the STLE/ASME Tribology Conference, Seattle, WA, October 1–4, 2000.

[12] Shampine, L. F., 1994, *Numerical Solution of Ordinary Differential Equations*, Chapman and Hall, New York.

[13] Green, I., and Etsion, I., 1986, ''Pressure and Squeeze Effects on the Dynamic Characteristics of Elastomer O-Rings Under Small Reciprocating Motion,'' ASME J. Tribol., **108**, No. 3, pp. 439–445.

[14] Lee, A. S., and Green, I., 1995, ''Physical Modeling and Data Analysis of the Dynamic Response of a Flexibly Mounted Rotor Mechanical Seal,'' ASME J. Tribol., **117**, pp. 130–135.

[15] Gross, W. A., 1980, *Fluid Film Lubrication*, John Wiley & Sons, New York.

[16] Green, I., 1987, ''The Rotor Dynamic Coefficients of Coned-Face Mechanical Seals with Inward or Outward Flow,'' ASME J. Tribol., **109**, No. 1, pp. 129–135.